

1 The diurnal cycle of the clouds extending above the tropical 2 tropopause observed by spaceborne lidar

3 Dauhut, Thibaut (1), Vincent Noel (2) and Iris-Amata Dion (3)

4 1. Max Planck Institute for Meteorology, Hamburg, Germany

5 2. Laboratoire d'Aérodologie, Université de Toulouse, CNRS, UPS, Toulouse, France

6 3. CRNM, Météo-France – CNRS, Toulouse, 31057, France

7 Proposed for publication in Atmospheric Chemistry and Physics

8 Contact author : T. Dauhut thibaut.dauhut@mpimet.mpg.de

9 Abstract

10 The presence of clouds above the tropopause over tropical convection centers has so far been
11 documented by spaceborne instruments that are either sun-synchronous, or insensitive to thin
12 cloud layers. Here we document, for the first time through direct observation by spaceborne lidar,
13 how the tropical cloud fraction evolves above the tropopause throughout the day. After confirming
14 previous studies that found such clouds are most frequent above convection centers, we show that
15 stratospheric clouds and their vertical extent above the tropopause follow a diurnal rhythm linked
16 to convective activity. The diurnal cycle of the stratospheric clouds displays two maxima: one in the
17 early night (19-20LT) and a later one (00-01LT). Stratospheric clouds extend up to 0.5-1km above
18 the tropopause during nighttime, when they are the most frequent. The frequency and the vertical
19 extent of stratospheric clouds is very limited during daytime, and when present they are found
20 very close to the tropopause. Results are similar over the major convection centers (Africa, South
21 America, Warm pool), with more clouds above land in DJF and less above ocean and JJA.

22 1. Scientific context and objectives

23 Low-stratospheric clouds impact the atmospheric system in several ways. First, their larger heating
24 rate than the clear sky (Corti et al, 2006) increases the upward mass flux and fosters the large-scale
25 upward transport of water above the tropopause. At the hour timescale, the cloud particles
26 penetrating the stratosphere via overshooting convection leads, on the one hand, to a direct
27 stratospheric humidification (Schoeberl et al., 2018; Dauhut et al., 2018). On the other hand, these
28 particles can serve as support for ice-scavenging: under saturated conditions, the water vapor
29 deposits on the particles, which grow and fall out (Corti et al., 2008), decreasing low-stratosphere
30 humidity (Jensen et al., 2013). By all these effects the stratospheric clouds modulate the
31 stratospheric water vapor concentrations (Iwasaki et al., 2015) and affect the overall dynamical
32 structure near the tropopause (Corti et al., 2006), at timescales down to one hour. This is why it is
33 important to understand the formation and the sub-daily evolution of such clouds.

34 The presence of ice clouds near the tropical tropopause has long been documented by in-situ
35 measurements (e.g. Thomas et al., 2002; Jensen et al., 2013; Frey et al., 2014). Detecting
36 occurrences of clouds extending above the tropopause by remote sensing requires documenting
37 the vertical cloud profile with a fine resolution and a high sensitivity to optically thin clouds, which
38 few instruments can reach. Lidar measurements are able to document such occurrences (e.g. Nee
39 et al., 1998; Dupont et al., 2010; Gouveia et al., 2017), but for a long time were limited to local
40 case studies. Dessler (2009) was the first to use the cloud detections by the CALIPSO lidar (Cloud-
41 Aerosol Lidar Infrared Pathfinder Satellite Observations) to investigate how clouds extend above
42 the tropopause on a global scale. Pan and Munchak (2011) refined the results by using an
43 advanced tropopause dataset. Both studies found that clouds extending into the stratosphere are
44 frequent above seasonal deep convection centers and rarely elsewhere, especially in midlatitudes.
45 Both studies deplored that the fixed overpass local time of the CALIPSO dataset is far from the late
46 afternoon, when land convection is at its maximum. More recently, Wang et al. (2019)

47 documented the presence of laminar cirrus in 10 years of CALIPSO data, and reported a non-
48 negligible cloud amount above the tropopause. Because of the sun-synchronous orbit of CALIPSO,
49 none of these studies were able to document the diurnal cycle of the stratospheric clouds.

50 The diurnal evolution of the high-altitude cirrus clouds have been documented over some specific
51 sites using ground-based lidars (Sassen et al. 2003; Dupont et al., 2010; Gouveia et al. 2017).
52 Gouveia et al. (2017) documented the evolution of the integrated cloud fraction (no vertical
53 distribution) over Amazonia, Sassen et al. (2003) documented the diurnal evolution of the
54 composition of cirrus clouds over Salt Lake City, and Dupont et al. (2010) did the same over four
55 observatories in France and in the United-States. However, using ground-based lidar to document
56 optically thin clouds extending above the tropopause is difficult for two reasons: 1) as the studies
57 based on CALIPSO observations show, these clouds occur primarily in regions where operational
58 ground-based sites are absent or very few (Pacific ocean, equatorial Africa, South America), and 2)
59 these clouds are mainly associated with deep convection, which implies the presence of optically
60 thick cloud systems in the troposphere beneath that will make in most cases impossible the
61 successful probing of optically thin clouds near the tropopause due to the attenuation of lidar
62 signal. This explains why the ground-based lidars do not document the diurnal cycle of the
63 stratospheric clouds with a satisfying spatial and temporal coverage.

64 Describing the diurnal evolution of the high-altitude clouds from a global perspective becomes
65 possible with the CATS (Cloud-Aerosol Transport System) lidar operated from the International
66 Space Station (ISS) between February 2015 and November 2017 (McGill et al., 2015). Thanks to the
67 ISS non-synchronous orbit, CATS was able to probe the vertical cloud distribution of a particular
68 region at different times of the day (not only at 0130 and 1330 Local Time like the instruments on
69 CALIPSO). Aggregating CATS detections over a region of interest and over enough time provides a
70 statistical overview of the diurnal evolution of cloud vertical profiles over that region (Noel et al.,

71 2018). Our work aims at using CATS observations to describe and understand better the diurnal
72 evolution of the cloud fraction in the tropical stratosphere.

73 Finding the processes responsible for the formation of tropical stratospheric clouds proves difficult,
74 just like with high-tropospheric clouds (Reverdy et al., 2012). Two processes have been mainly
75 proposed. Overshooting convection can lead to the injection of ice crystals into the stratosphere
76 (Dauhut et al., 2018; Lee et al., 2018). Stratospheric cooling triggered by gravity waves (Pfister et
77 al., 2010) could also lead to so-called cloud “in-situ” formation (Pan and Munchak, 2011). The ratio
78 of stratospheric clouds that are formed in-situ has not been estimated yet. The current study does
79 not provide further estimate, but by describing the spatio-temporal evolution of the stratospheric
80 clouds, it highlights how important the convective activity is to drive the stratospheric cloudiness,
81 and how the twice-daily sampling by lidars onboard sun-synchronous platforms can miss the
82 highest and largest stratospheric cloud fraction over certain regions.

83 In this paper, we document for the first time the diurnal cycle of clouds above the tropopause in
84 the Tropics, and the extent of their penetration in the stratosphere, thanks to the high vertical and
85 temporal resolution of the cloud detection by the CATS lidar. After describing CATS cloud data, and
86 the method to retrieve the tropopause heights used to detect clouds extending in the stratosphere
87 (Sect. 2), we present maps of stratospheric clouds and document their diurnal cycle in regions of
88 interest (Sect. 3). We then summarise our results and conclude (Sect. 4).

89 2. Data and Methods

90 2.1 CATS Cloud data

91 Between February 2015 and November 2017, the CATS lidar reported profiles at a vertical
92 resolution of 60m every 350m along-track, with an average repeat cycle of nearly 3 days (Yorks et
93 al., 2016). CATS Level 2 Operational layer files (L2O files, Palm et al., 2016) describe altitudes where
94 cloud layers were detected within profiles of backscatter coefficients measured at 1064nm by the
95 CATS lidar (Pauly et al., 2019), averaged 5km along-track. We considered all such files over the
96 CATS operation period and inspected each 5-km profile within. For profiles located in the Tropics
97 (30S-30N), we inspected each atmospheric layer therein identified as a cloud layer according to the
98 CATS layer type information. As in Noel et al. (2018), we considered layers with a Feature Type
99 Score above 6, to avoid any possibly mislabeled aerosol layers. We flagged the cloud layers with a
100 top altitude above the tropopause. Since any CATS L2O layer entirely above the tropopause is
101 labelled as an aerosol layer (like in CALIPSO, Pan and Munchak, 2011), our study will not include
102 clouds with their base in the stratosphere.

103 Davis et al (2010) noted that lidars in space may miss the thinnest subvisible cirrus clouds, but with
104 enough spatial averaging optical depths near 0.001 can be detected (Martins et al., 2011). Lidar
105 cloud detections also suffer from a lower sensitivity in the presence of sunlight, which induces
106 significant additional noise in the lidar signal, but climatologies are still relevant (Noel et al., 2018).

107 2.2. Tropopause Heights

108 To obtain the tropopause height, we considered profiles of temperature and pressure from the
109 ERA-5 reanalysis dataset (Albergel et al., 2018). These profiles are available every 6 hours, on 37
110 vertical levels and a 0.25° x 0.25° horizontal grid. Such profiles in ERA-5 reanalysis agree well with

111 observations in the high tropical troposphere (Podglajen et al. 2014). Using these profiles, we
112 computed the vertical lapse rate profile (as in Reichler et al. 2003), and interpolated it on a 100-m
113 vertical grid. We then applied the WMO criteria defining the presence of a tropopause -- i.e. the
114 lowest altitude at which the lapse rate falls below 2°C/km, provided the lapse-rate between this
115 altitude and all higher altitudes within 2 km does not exceed 2°C/km (WMO, 1957). Following the
116 WMO definition, we also allowed for the possibility of a second tropopause if the lapse rate
117 exceeds 3°C/km at least 1 km above the first tropopause. In such a case, we started to look for
118 another tropopause above. To limit computation overhead we constrained the search below 22
119 km. Using the WMO tropopause definition further allows us to compare our results to previous
120 efforts based on CALIPSO database that used the same definition (Pan and Munchak, 2011).

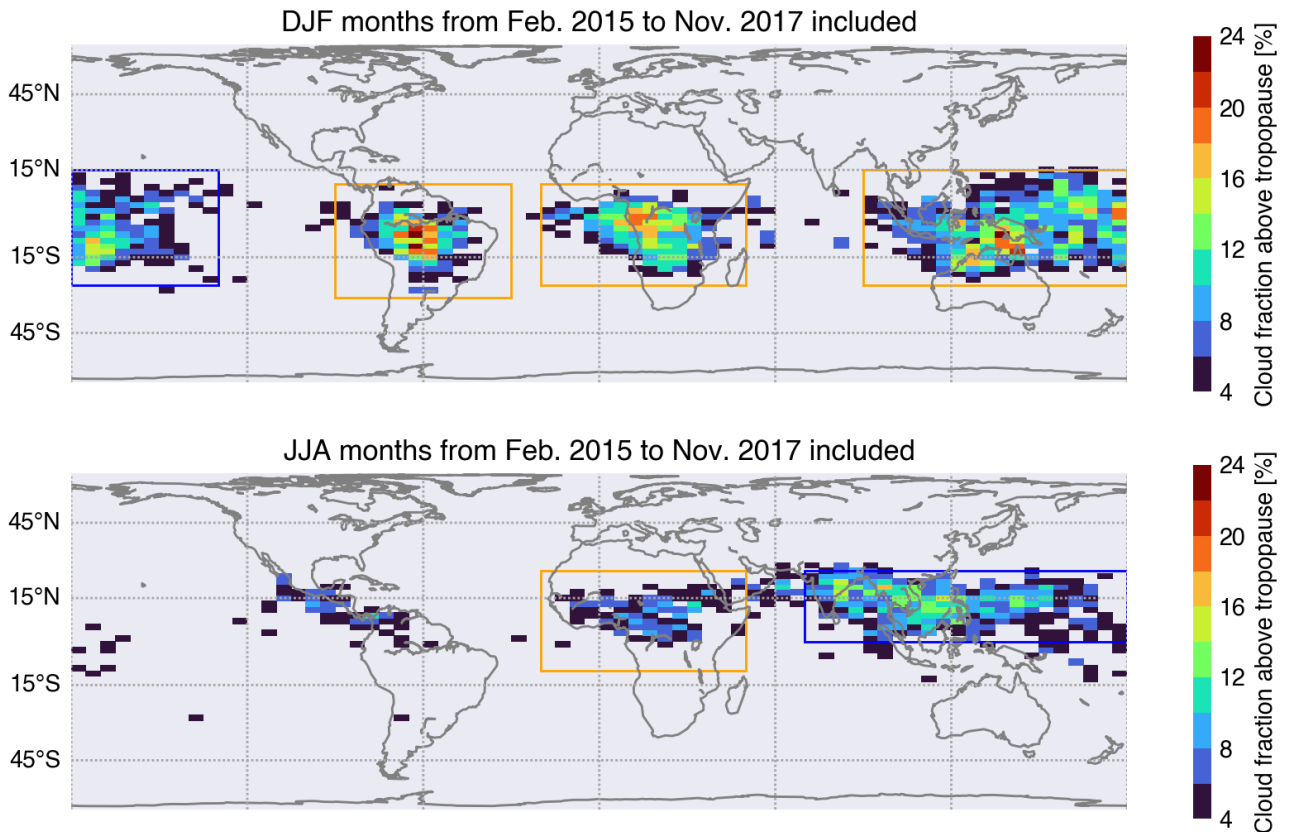
121 **2.3 Stratospheric cloud detection**

122 For a given CATS 5-km profile (Sect. 2.1), we identified the ERA-5 tropopause height (Sect. 2.2)
123 closest in time and location. Given the 6-hour time resolution of the ERA-5 reanalysis, there is at
124 most 3 hours difference between the observation time and the thermodynamic information used
125 to retrieve the tropopause height. We used the cloud information contained in the 5-km profiles in
126 two ways. First, in 2°x5° lat-lon bins we counted how many profiles contained a cloud extending
127 above the tropopause, compared to the total number of profiles in the bins. Aggregating such
128 numbers observed in JJA and DJF over the CATS operation period produced seasonal maps of
129 above-tropopause cloud amounts (Sect. 3.1). Second, from each CATS 5-km profile we built a
130 vertical cloud mask, using the tropopause height as the vertical reference and considering clouds
131 that extend above it. Within regions chosen based on the seasonal maps, we aggregated such
132 cloud masks over the same periods as above, keeping also track of the local time of observation for
133 the considered mask. This produced regional vertical cloud fraction profiles above the tropopause,
134 one profile for each local time of observation (Sect. 3.2).

135 3. Results

136 3.1 Stratospheric cloud distributions

137 Figure 1 shows the fraction of CATS profiles in which a cloud is detected above the tropopause, in
138 all DJF (top) and JJA (bottom) months of CATS operation.



139 **Figure 1:** Tropical low-stratosphere cloud fraction for (top) DJF and (bottom) JJA CATS
140 measurements between Feb 2015 and Nov 2017, calculated by considering all profiles in 2°x5° lat-
141 lon boxes. The rectangles are the regions in which cloud detections are aggregated in the rest of
142 the study. In DJF, from left to right : West Pacific (25S-15N, 180W-130W), South America (30S-10N,
143 90W-30W), Equatorial Africa (25S-10N, 20W-50E), and South Warm Pool (25S-15N, 90E-180E). In
144 JJA, from left to right : Central Africa (10S-25N, 20W-50E), North Warm Pool (0-25N, 70E-180E).
145 Only detections in the ±30° region are shown here. In the rest of the study, we considered profiles
146 over ocean in blue boxes and profiles over land in orange boxes.

147 Figure 1 shows that clouds in the tropical stratosphere are mostly detected over continents (South
148 America, Equatorial Africa and land masses in South Warm Pool in DJF; Central America, Central
149 Africa and land masses in North Warm Pool in JJA). The cloud fraction in the lower stratosphere is

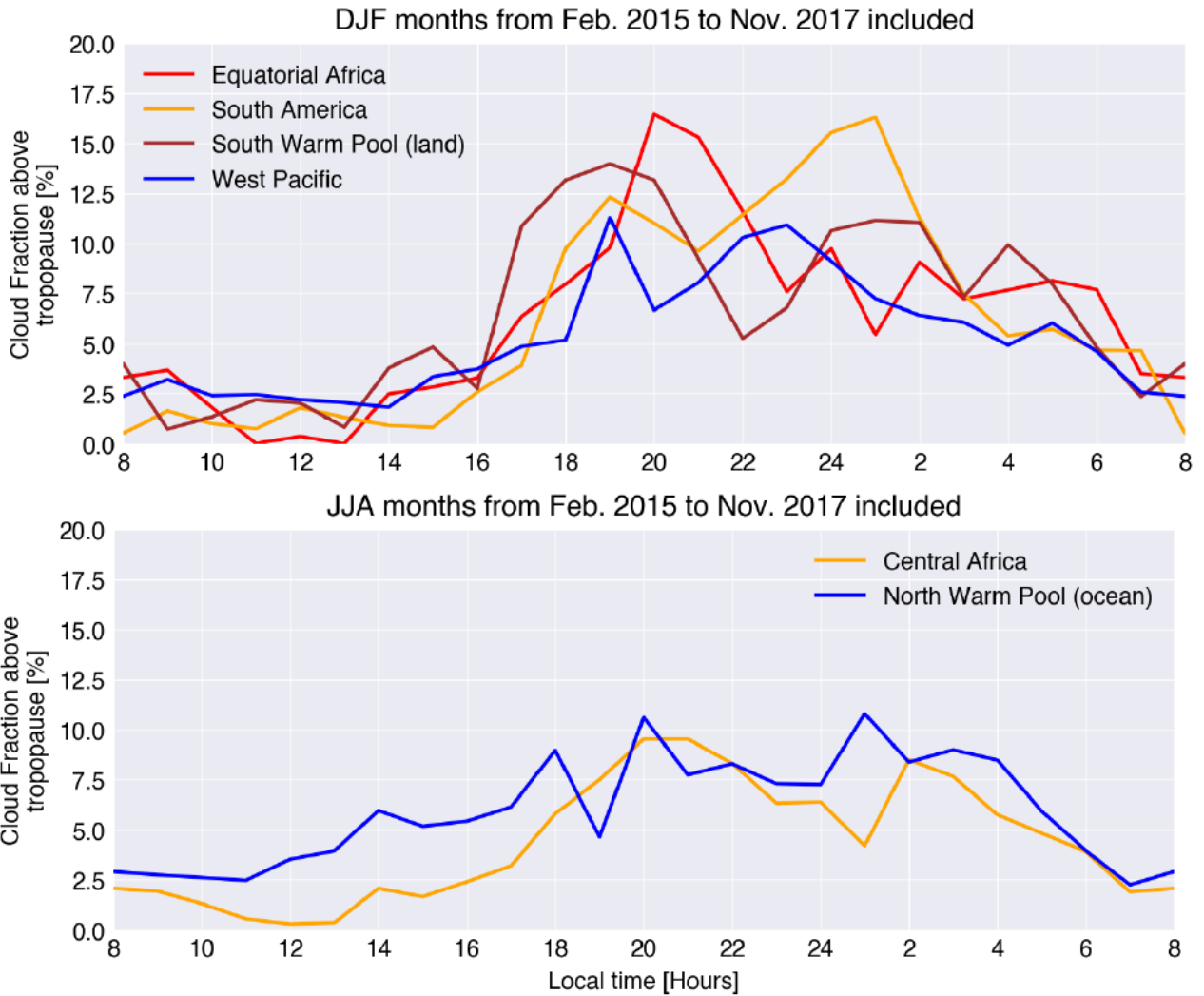
150 largest in DJF, up to 24% over central Amazonia and coastal areas in South Warm Pool, and up to
151 20% over Equatorial Africa. It is significantly lower in JJA, up to 12% over Africa and 16% over the
152 North Warm Pool, even though the lowermost stratosphere (380-420 K potential temperature) is
153 moister in JJA than in DJF (cf. e.g. Fig. 8c in Fueglistaler et al, 2009). Several factors may contribute
154 to this seasonal variation: the density and strength of the convective systems (Liu and Zipser,
155 2005), their propensity to propagate or to be stationary (Houze et al, 2015), the activity and
156 efficiency of the in situ formation processes (Jensen et al., 2001; Jensen and Pfister, 2004).

157 The spatio-temporal distribution of the stratospheric clouds is in very good agreement with the 4-
158 year climatology of Pan and Munchak (2011) from CALIPSO observations. The DJF distribution also
159 matches very well the CALIPSO cirrus detection at 100 hPa reported by Wang et al (2019) for
160 January 2009. We report though lower cloud frequencies than Wang et al. (2019) which can be
161 explained that we investigate slightly higher altitudes. Both CATS and CALIPSO datasets find 1)
162 significantly weaker stratospheric cloud fraction in JJA than in DJF, and 2) near-zero stratospheric
163 clouds in the subtropics. These results are also consistent with the CALIPSO cloud fractions near
164 16km reported by Schoeberl et al. (2019). Since those studies consider cloud detections derived
165 from a spaceborne lidar instrument, over several years for most, their good agreement suggests
166 that the CATS stratospheric cloud detections at 1064 nm are as reliable as the CALIPSO ones at 532
167 nm. A first conclusion of our results is therefore that CATS measurements strongly support the
168 findings of all other studies using detections of high clouds from CALIPSO data.

169 Our CATS results are also in very good agreement with the distributions of clouds near the
170 tropopause from other space instruments: 2006-2007 HIRDLS (High Resolution Dynamics Limb
171 Sounder) reported by Massie et al. (2010), 2006-2014 CloudSat observations (Kim et al., 2018),
172 and the pioneering 1989 passive Stratospheric Aerosol and Gas Experiment (SAGE) II observations
173 (Jensen et al., 1996). Besides the specificity in the cloud detection method employed by each
174 instrument (occultation for HIRDLS and SAGE II, radar backscattering for CloudSat), the little

175 differences between the distributions mostly come from the year-to-year variability. Larger
176 differences can be found with the distributions of clouds penetrating the tropical tropopause
177 derived from the 1998-2000 and 2002-2003 observations by the Tropical Rainfall Measuring
178 Mission (TRMM) Precipitation Radar (Liu and Zipser, 2005). The densities of overshooting systems
179 with tops in the lower stratosphere (on which Liu and Zipser (2005) focused rather than all
180 stratospheric clouds) are remarkably larger in Central America and Central Africa than over the
181 Warm Pool. Since TRMM precipitation radar reflectivities are less sensitive to thin ice particles than
182 CATS and CALISPO lidars, we can interpret this difference by the fact that the American and African
183 systems, though frequently overshooting the stratosphere, produce less thin stratospheric clouds
184 than the Asian systems, or other in-situ processes (like gravity wave cooling) are more efficient to
185 produce stratospheric clouds over Asia than America and Africa.

186 **3.2 Diurnal cycle of cloud fractions in the tropical stratosphere**



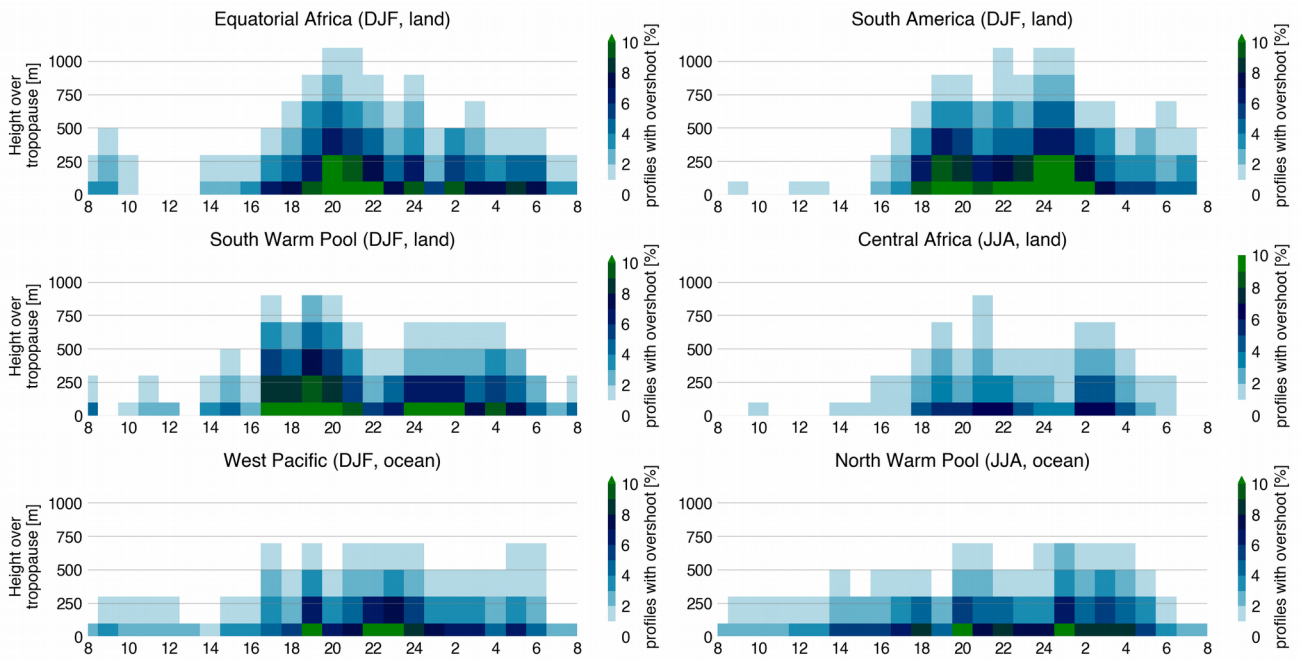
187 **Figure 2:** Diurnal cycle of stratospheric cloud fraction, by tropical region as in Fig. 1, averaged over
 188 DJF (top) and JJA (bottom).

189 In contrast with the previous studies, the CATS dataset allows us to analyse the diurnal cycle of the
 190 cloud fraction in stratosphere. The cloud fraction at regional scale shows a consistent diurnal cycle,
 191 robust over the different regions identified in the previous section (Fig. 2). In particular and in
 192 contrast to the diurnal cycle of surface precipitation, there is no land-ocean difference. All exhibit a
 193 pronounced minimum about 2-4 % during the day time, from 7 to 16 LT. They all present a first
 194 maximum at 19 or 20 LT (early-night peak), up to 16.5% over Equatorial Africa. For all regions
 195 except South America and North Warm Pool, this maximum is the largest cloud fraction of the day.
 196 All regions also present a second peak (late-night peak) at 0 or 1 LT (23 LT for West Pacific and 2 LT
 197 for Central Africa), up to 16.5% over South America. The midnight peak over Equatorial Africa is

198 less clear than over the other regions because of the large variations between 23 and 3 LT. The
199 capability of a longer dataset to produce a clearer signal is to be investigated.

200 The cirrus clouds observed over Amazonia by ground-based lidar (Gouveia et al., 2017) shows a
201 very similar diurnal cycle: a first peak in the early night (at 18-19 LT), a second peak later in the
202 night (at 2-3 LT). Although Gouveia et al. (2017) do not consider the cloud above the tropopause
203 only, their distinction between subvisible, thin and opaque cirrus indicates that the opaque cirrus
204 are predominant during the early night (18-21 LT) and the thin cirrus (and subvisible ones during
205 the dry season) dominate during the later night (from 0 and 2 LT onward, in wet and dry seasons,
206 respectively).

207 The very deep convection transports cloudy air masses beyond the tropopause via overshoots and
208 then directly contributes to the stratospheric cloud fraction (Dauhut et al., 2016 and 2018). The
209 diurnal cycle of the stratospheric cloud fraction observed by CATS can at the first order be
210 explained by the diurnal cycle of very deep convection over land (Liu and Zipser, 2005), especially
211 (i) the minimal value during daytime, and (ii) the first peak in the early evening. This first peak
212 occurs with a delay of 3 to 4 hours compared to the very deep convection maximum. As the
213 dataset used by Liu and Zipser (2005) is more sensitive to overshoots freshly developed into the
214 stratosphere, this delay can be explain by the subsequent horizontal expansion of the overshoots
215 and their spread by the winds (Dauhut et al., 2018; Lee et al., 2019). The convective generation of
216 gravity waves, that produce transient cooling off the convective centres and in some conditions
217 trigger cloud formation, can also contribute to the increase of the stratospheric cloud fraction after
218 the maximum of the very deep convection, and then explain the delay of the first peak and
219 potentially the second peak. It may also explain the similar diurnal cycle over the ocean regions,
220 either close (South Warm Pool Ocean) or remote (West Pacific) from land masses. This process
221 remains to be investigated.



222 **Figure 3:** Diurnal cycle of cloud fraction as a function of height above the tropopause, by tropical
 223 region as in Fig. 1, in DJF (top 2 rows) and JJA (bottom row).

224 Figure 3 shows how far above the tropopause the clouds extend, depending on the local time in
 225 each tropical region (Sect. 3.1). Some regions are considered in DJF, others in JJA, because the
 226 stratospheric cloud distribution changes throughout the year (Fig. 1), following the ITCZ position.
 227 Patterns appear very consistent in all the regions considered. In all regions the largest cloud
 228 fractions are found near the tropopause, with few clouds extending higher. Cloud fractions extend
 229 relatively high (up to 1km above the tropopause) during the early night. The first peak of cloud
 230 fraction, near 19-20LT (Fig. 2), is associated with the all-day maximum of cloud vertical extent, with
 231 clouds in 5% of profiles reaching 1km above the tropopause in DJF regions. During the rest of the
 232 night (after 00 LT) clouds are still present but extend less high (except over South America). During
 233 daytime (0600-1800) clouds appear very close to the tropopause. Cloud fractions are overall much
 234 smaller in JJA (max 5-10%, bottom row) than in DJF (max 10-12%, rows 1 and 2).

235 In addition to describing the evolution of the stratospheric cloud cover at hourly timescales, these
 236 observations help interpret observations with limited temporal sampling (Noel et al., 2018). The

237 Microwave Limb Sounder (MLS), like CALIPSO and all other instruments onboard platforms of the
238 A-Train, samples the atmosphere at 01:30 and 13:30 LT, providing one single night and one single
239 day observation. Some authors (e.g., Dion et al., 2019) attempt to retrieve the diurnal cycle of the
240 observed water contents in the tropopause region, combining MLS observations with higher
241 temporal resolution observation of convective activity based on TRMM observation of
242 precipitation. Dion et al. (2019) assumed an in-phase relationship between precipitation and ice
243 water content in the upper troposphere and at the tropopause level. For the stratospheric ice
244 water content, MLS data still provides a too low signal-to-noise ratio. For future investigations, our
245 results indicate that the stratospheric cloud fraction at 13:30 LT is, whatever the region, close to
246 the minimal value of its diurnal cycle, whereas at 01:30 LT it is more typical of the second
247 maximum. Carminati et al. (2014) investigated, from MLS measurements between 2005 and 2012,
248 the differences between day and night ice water contents in the upper troposphere and the
249 tropopause level. Unlike the stratospheric cloud fraction, tropopause ice water contents are larger
250 at 13:30 LT than at 01:30 LT over Equatorial Africa during DJF, Central Africa during JJA, and over
251 South America during both seasons. A possible explanation to reconcile our results is that
252 tropopause ice water content is more sensitive to fresh convective activity (very deep convection
253 occurrence) whereas the stratospheric cloud cover is more sensitive to the diffusion of the injected
254 ice in the stratosphere.

255 **4. Conclusion**

256 Our results show how clouds in the tropical stratosphere are strongly concentrated above deep
257 convection centers, are almost absent in subtropical regions, are more frequent in DJF than JJA,
258 and over land than over ocean. In addition to these results, which are consistent with most
259 previous studies, we also show that both the cloud fraction and its extension above the
260 tropopause follow a diurnal rhythm with a maximum during the early nighttime and a near-zero
261 minimum during daytime. During daytime, the stratospheric clouds are limited to the first hundred
262 meters above the tropopause. During nighttime, significant average cloud fraction is found up to 1
263 km above the tropopause. A second maximum of stratospheric cloud fraction is observed over all
264 regions, generally little after midnight. These results highlight how much the evolution of
265 stratospheric clouds can be undersampled by other spatial instruments restricted to 01:30 and
266 13:30 LT, that then miss for instance the first maximum and the deepest development of
267 stratospheric clouds in the early night. The very deep convective activity over tropical lands drives
268 most of this diurnal cycle, and leads in particular to the minimal stratospheric cloud fraction during
269 daytime and the second peak during nighttime, both consistent over all regions. Further
270 investigation is though necessary to describe how convection contributes to this diurnal cycle, and
271 to assess the role of other processes leading to stratospheric cloud formation like the gravity
272 waves. Finally further research is needed to understand why the timing of this diurnal cycle is very
273 similar over land and over ocean.

274 **Author contribution.** TD and VN designed the data analyses and VN carried them out. TD
275 prepared the manuscript with contributions from VN and ID.

276 **Acknowledgments.** The authors would like to thank B. Legras (LMD) and F. Pantillon (LA) for
277 useful discussions on the quality of tropopause altitudes from various sources. They also thank

278 NASA EarthData for access to CATS data and ECMWF for access to the ERA5 reanalysis dataset. This
279 research was supported by the IDEX TEASAO project. Primary data and scripts used in the analysis
280 and other supplementary information that may be useful in reproducing the author's work are
281 archived by the Max Planck Institute for Meteorology and can be obtained by contacting
282 publications@mpimet.mpg.de

283 References

- 284 • Albergel, C., Dutra, E., Munier, S., Calvet, J.-C., Munoz-Sabater, J., de Rosnay, P., and
285 Balsamo, G.: ERA-5 and ERA-Interim driven ISBA land surface model simulations: which one
286 performs better?, *Hydrol. Earth Syst. Sci.*, 22, 3515-3532, [https://doi.org/10.5194/hess-22-](https://doi.org/10.5194/hess-22-3515-2018)
287 [3515-2018](https://doi.org/10.5194/hess-22-3515-2018), 2018.
- 288 • Carminati, F., Ricaud, P., Pommereau, J.-P., Rivière, E., Khaykin, S., Attié, J.-L., and Warner, J.:
289 Impact of tropical land convection on the water vapour budget in the tropical tropopause
290 layer, *Atmos. Chem. Phys.*, 14, 6195-6211, <https://doi.org/10.5194/acp-14-6195-2014>,
291 2014.
- 292 • Corti, T., Luo, B. P., Fu, Q., Vömel, H., and Peter, T.: The impact of cirrus clouds on tropical
293 troposphere-to-stratosphere transport, *Atmos. Chem. Phys.*, 6, 2539-2547,
294 <https://doi.org/10.5194/acp-6-2539-2006>, 2006.
- 295 • Corti, T., et al.: Unprecedented evidence for deep convection hydrating the tropical
296 stratosphere, *Geophys. Res. Lett.*, 35, L10810, <https://doi.org/10.1029/2008GL033641>,
297 2008.
- 298 • Dauhut, T., Chaboureau, J., Haynes, P.H., and Lane, T.P.: The Mechanisms Leading to a
299 Stratospheric Hydration by Overshooting Convection, *J. Atmos. Sci.*, 75, 4383-4398,
300 <https://doi.org/10.1175/JAS-D-18-0176.1>, 2018.
- 301 • Davis, S., et al.: In situ and lidar observations of tropopause subvisible cirrus clouds during
302 TC4, *J. Geophys. Res.*, 115, D00J17, <https://doi.org/doi:10.1029/2009JD013093>, 2010.

- 303 • Dessler, A. E.: Clouds and Water Vapor in the Northern Hemisphere Summertime
304 Stratosphere, 114, *J. Geophys. Res.*, 114, <https://doi.org/10.1029/2009JD012075>, 2009.
- 305 • Dion, I. A., Ricaud, P., Haynes, P., Carminati, F., and Dauhut, T.: Ice injected into the
306 tropopause by deep convection – Part 1: In the austral convective tropics, *Atmos. Chem.*
307 *Phys.*, 19(9), 6459-6479, <https://doi.org/10.5194/acp-19-6459-2019>, 2019.
- 308 • Frey, W., Borrmann, S., Fierli, F., Weigel, R., Mitev, V., Matthey, R., Ravegnani, F., Sitnikov, N.
309 M., Ulanovsky, A., and Cairo, F.: Tropical deep convective life cycle: Cb-anvil cloud
310 microphysics from high-altitude aircraft observations, *Atmos. Chem. Phys.*, 14, 13223-
311 13240, <https://doi.org/10.5194/acp-14-13223-2014>, 2014.
- 312 • Houze, R. A., Rasmussen, K. L., Zuluaga, M. D., and Brodzik, S. R.: The variable nature of
313 convection in the tropics and subtropics: A legacy of 16 years of the Tropical Rainfall
314 Measuring Mission satellite, *Rev. Geophys.*, 53, 994–1021,
315 <https://doi.org/10.1002/2015RG000488>, 2015.
- 316 • Iwasaki, S., Luo, Z. J., Kubota, H., Shibata, T., Okamoto, H., and Ishimoto, H.:
317 Characteristics of cirrus clouds in the tropical lower stratosphere, *Atmos. Res.*, 164–165,
318 358–368, <https://doi.org/10.1016/j.atmosres.2015.06.009>, 2015.
- 319 • Jensen, E. J., Toon, O. B., Selkirk, H. B., Spinhirne, J. D., and Schoeberl, M. R.: On the
320 formation and persistence of subvisible cirrus clouds near the tropical tropopause, *J.*
321 *Geophys. Res.*, 101(D16), 21361– 21375, <https://doi.org/10.1029/95JD03575>, 1996.
- 322 • Jensen, E. J., Pfister, L., Ackerman, A. S., Tabazadeh, A., and Toon, O. B.: A conceptual model
323 of the dehydration of air due to freeze-drying by optically thin, laminar cirrus rising slowly
324 across the tropical tropopause, *J. Geophys. Res.*, 106(D15), 17237– 17252,
325 <https://doi.org/10.1029/2000JD900649>, 2001.
- 326 • Jensen, E., and Pfister, L.: Transport and freeze-drying in the tropical tropopause layer, *J.*
327 *Geophys. Res.*, 109, D02207, <https://doi.org/10.1029/2003JD004022>, 2004.
- 328 • Jensen, E. J., Diskin, G., Lawson, R. P., Lance, S., Bui, T. P., Hlavka, D., McGill, M., Pfister, L.,
329 Toon, O. B., and Gao, R.: Ice nucleation and dehydration in the Tropical Tropopause Layer,
330 *PNAS*, 110, 2041–2046, doi:10.1073/pnas.1217104110, 2013.

- 331 • Kim, J., Randel, W. J., and Birner, T.: Convectively driven tropopause-level cooling and its
332 influences on stratospheric moisture, *J. Geophys. Res.-Atmos.*, 123, 590– 606,
333 <https://doi.org/10.1002/2017JD027080>, 2018.
- 334 • Lee, K.-O., Dauhut, T., Chaboureau, J.-P., Khaykin, S., Krämer, M., and Rolf, C.: Convective
335 hydration in the tropical tropopause layer during the StratoClim aircraft campaign: Pathway
336 of an observed hydration patch, *Atmos. Chem. Phys.*, [https://doi.org/10.5194/acp-2018-](https://doi.org/10.5194/acp-2018-1114)
337 [1114](https://doi.org/10.5194/acp-2018-1114), 2019.
- 338 • Liu, C., and Zipser, E. J.: The global distribution of largest, deepest, and most intense
339 precipitation systems, *Geophys. Res. Lett.*, 42, 3591– 3595,
340 <https://doi.org/10.1002/2015GL063776>, 2005.
- 341 • Martins, E., Noel, V., and Chepfer, H.: Properties of cirrus and subvisible cirrus from
342 nighttime Cloud-Aerosol Lidar with Orthogonal Polarization (CALIOP), related to
343 atmospheric dynamics and water vapor, *J. Geophys. Res.*, 116, D02208,
344 <https://doi.org/10.1029/2010JD014519>, 2011.
- 345 • Massie, S. T., Gille, J., Craig, C., Khosravi, R., Barnett, J., Read, W., and Winker, D.: HIRDLS
346 and CALIPSO observations of tropical cirrus, *J. Geophys. Res.*, 115, D00H11,
347 <https://doi.org/10.1029/2009JD012100>, 2010.
- 348 • McGill, M. J., Yorks, J. E., Scott, V. S., Kupchock, A. W., and Selmer, P. A.: The Cloud-Aerosol
349 Transport System (CATS): A technology demonstration on the International Space Station,
350 *Proc. SPIE 9612, Lidar Remote Sensing for Environmental Monitoring XV*, 96120A,
351 <https://doi.org/10.1117/12.2190841>, 2015.
- 352 • Nee, J. B., Len, C. N., Chen, W. N., and Lin, C. I.: Lidar observation of the cirrus cloud in the
353 tropopause at Chung Li (25°N, 121°E), *J. Atmos. Sci.*, 55, 2249– 2257, 1998.
- 354 • Noel, V., Chepfer, H., Chiriaco, M., and Yorks, J.: The diurnal cycle of cloud profiles over land
355 and ocean between 51° S and 51° N, seen by the CATS spaceborne lidar from the
356 International Space Station, *Atmos. Chem. Phys.*, 18, 9457-9473,
357 <https://doi.org/10.5194/acp-18-9457-2018>, 2018.

- 358 • Palm, S. P., Hlavka, D. L., Selmer, P., and Pauly, R.: the Cloud Aerosol Transport System (CATS)
 359 Data Product Catalog release 3.0, available at: [https://cats.gsfc.nasa.gov/media/docs/CATS_](https://cats.gsfc.nasa.gov/media/docs/CATS_Data_Products_Catalog.pdf)
 360 [Data_Products_Catalog.pdf](https://cats.gsfc.nasa.gov/media/docs/CATS_Data_Products_Catalog.pdf) (last access: 23 January 2018), 2016.
- 361 • Pan, L. L., and Munchak, L. A.: Relationship of Cloud Top to the Tropopause and Jet
 362 Structure from CALIPSO Data, *J. Geophys. Res.*, 116, D12201,
 363 <https://doi.org/10.1029/2010JD015462>, 2011.
- 364 • Pauly, R. M., Yorks, J. E., Hlavka, D. L., McGill, M. J., Amiridis, V., Palm, S. P., Rodier, S. D.,
 365 Vaughan, M. A., Selmer, P. A., Kupchock, A. W., Baars, H., and Gialitaki, A.: Cloud Aerosol
 366 Transport System (CATS) 1064 nm Calibration and Validation, *Atmos. Meas. Tech. Discuss.*,
 367 <https://doi.org/10.5194/amt-2019-172>, 2019
- 368 • Pfister, L., Selkirk, H. B., Starr, D. O., Rosenlof, K., and Newman, P.A.: A meteorological
 369 overview of the TC4 mission, *J. Geophys. Res.*, 115, D00J12,
 370 <https://doi.org/10.1029/2009JD013316>, 2010.
- 371 • Podglajen, A., Hertzog, A., Plougonven, R., and Žagar, N.: Assessment of the accuracy of
 372 (re)analyses in the equatorial lower stratosphere, *J. Geophys. Res. Atmos.*, 119, 11166–
 373 11188, <https://doi.org/10.1002/2014JD021849>, 2014.
- 374 • Reichler, T., Dameris, M., and Sausen, R.: Determining the Tropopause Height from Gridded
 375 Data, *Geophys. Res. Lett.*, 30, 2042, <https://doi.org/10.1029/2003GL018240>, 2003.
- 376 • Reverdy, M., Noel, V., Chepfer, H., and Legras, B.: On the origin of subvisible cirrus clouds in
 377 the tropical upper troposphere, *Atmos. Chem. Phys.*, 12, 12081-12101,
 378 <https://doi.org/10.5194/acp-12-12081-2012>, 2012.
- 379 • Schoeberl, M. R., Jensen, E. J., Pfister, L., Ueyama, R., Wang, T., Selkirk, H., et al.: Water
 380 vapor, clouds, and saturation in the tropical tropopause layer. *J. Geophys. Res.-Atmos.*, 124,
 381 3984– 4003, <https://doi.org/10.1029/2018JD029849>, 2019.
- 382 • Thomas, A., Borrmann, S., Kiemle, C., Cairo, F., Volk, M., Beuermann, J., Lepuchov, B.,
 383 Santacesaria, V., Matthey, R., Rudakov, V., Yushkov, V., MacKenzie, A. R., and Stefanutti,

- 384 L.: In situ measurements of background aerosol and subvisible cirrus in the tropical
385 tropopause region, *J. Geophys. Res.*, 107, 4763, doi:10.1029/2001JD001385, 2002.
- 386 • Wang, T., Wu, D. L., Gong, J., and Tsai, V.: Tropopause laminar cirrus and its role in the lower
387 stratosphere total water budget. *J. Geophys. Res.-Atmos.*, 124, 7034– 7052,
388 <https://doi.org/10.1029/2018JD029845>, 2019.
- 389 • Yorks, J. E., McGill, M. J., Palm, S. P., Hlavka, D. L., Selmer, P. A., Nowottnick, E. P., Vaughan,
390 M. A., Rodier, S. D., and Hart, W. D.: An overview of the CATS level 1 processing algorithms
391 and data products, *Geophys. Res. Lett.*, 43, 4632– 4639,
392 <https://doi.org/10.1002/2016GL068006>, 2016.